Nonlinear Dyn (2023) 111:19347–19357
https://doi.org/10.1007/s11071-023-08843-7

ORIGINAL PAPER

Nth order generalized Darboux transformation and solitons, breathers and rogue waves in a variable-coefficient coupled nonlinear Schrödinger equation

N. Song · R. Liu · M. M. Guo · W. X. Ma

Received: 24 May 2023 / Accepted: 5 August 2023 / Published online: 4 September 2023

Abstract Based on the generalized Darboux transformation, the underlying propagation mechanism of localized waves is systematically studied. More specifically, the variable-coefficient coupled nonlinear Schrödinger (NLS) equation is used to accurately describe the dispersion compensation and lumped amplification properties in an inhomogeneous optical fiber. Based on the Lax pair and the seed solutions, the expressions of both the first- and second-order localized wave solutions are calculated. Then, by performing numerical simulations, the evolutionary plots of the interaction of rogue waves with bright-dark solitons and breathers are obtained, and their dynamical characteristics are further analyzed. From the acquired results, it is found that the values of $\beta\ (z)$ and $\gamma\ (z)$ have a direct influence on the propagation shape of the localized waves. Our work provides valuable insights into the dynamical characteristics of the localized waves that the variable-coefficient equations could describe to a certain extent.

Keywords Variable-coefficient coupled NLS equation · Bright-dark solitons · Breathers · Rogue waves · Generalized Darboux transformation

N. Song (✉) · R. Liu · M. M. Guo
Department of Mathematics, North University of China, Taiyuan 030051, Shanxi, China
e-mail: songni@nuc.edu.cn

W. X. Ma
Department of Mathematics, Zhejiang Normal University, Jinhua 321004, Zhejiang, China

W. X. Ma
Department of Mathematics, King Abdulaziz University, Jeddah 21589, Saudi Arabia

W. X. Ma
Department of Mathematics and Statistics, University of South Florida, Tampa, FL 33620-5700, USA

W. X. Ma (✉)
School of Mathematical and Statistical Sciences, North-West University, Mafikeng Campus, Private Bag X2046, Mmabatho 2735, South Africa
e-mail: mawx@cas.usf.edu

1 Introduction

As is well-established, the nonlinear Schrödinger (NLS) equation is regarded as one of the most fundamental and important equations in the field of nonlinear science [1,2]. Generally, it can accurately describe the properties of nonlinear waves in physical systems, and also simulate the transmission of light in optical fibers [3–5]. In addition, it is widely utilized in many branches of applied mathematics and physics including quantum theory [6,7], condensed matter physics [8], and optical fiber communication [9,10]. In recent years, with the wide implementation of the NLS equations by many works in the literature, it has been found that as both time and space are changed, the constant coefficient NLS equations can only approximate the law of material motion change. As a result, to more accurately reflect the complex motion change law that takes place in the real world, it is necessary to establish the

variable-coefficient NLS equations [11,12]. Moreover, such type of equations has been already applied to describe the localized waves, which consist of solitons [13,14], breathers [15], and rogue waves [16]. Several methods for studying the localized wave solutions have been proposed in the literature including the generalized Darboux transformation [17,18], the Bäcklund transformation [19], the inverse scattering transformation [20], the Hirota bilinear method [21], and the Riemann-Hilbert method [22]. Therefore, by using the variable-coefficient NLS equations, a large number of complex nonlinear phenomena have been successfully explained, whereas the development of nonlinear fields has been also significantly promoted.

Based on the above-mentioned considerations, a variable-coefficient coupled NLS equation was thoroughly studied. Particularly, a two-channel wavelength division multiplexed soliton structure coupled with the dispersion compensation and lumped amplification in an inhomogeneous optical fiber was analyzed as follows [23]:

$$iq_{1z}+\tfrac{\beta(z)}{2}q_{1tt}+\gamma(z)\left(|q_1|^2+|q_2|^2\right)q_1+i\delta(z)q_1=0, \tag{1a}$$

$$iq_{2z}+\tfrac{\beta(z)}{2}q_{2tt}+\gamma(z)\left(|q_1|^2+|q_2|^2\right)q_2+i\delta(z)q_2=0, \tag{1b}$$

where q_1 and q_2 represent the two polarized components of the propagating electromagnetic waves, z and t denote the partial derivative of the coordinates along with the direction of the wave propagation, $\gamma(z)$ refers to the coefficient of self-phase modulation (SPM) and cross-phase modulation (XPM) of nonlinear effects, and $\beta(z)$ and $\delta(z)$ stand for the group velocity dispersion (GVD) and amplification or absorption coefficients, respectively. Besides, it was found that Eqs. (1a) and (1b) are integrable when $\delta(z)=\frac{\gamma_z(z)\beta(z)-\gamma(z)\beta_z(z)}{2\beta(z)\gamma(z)}$.

The above-mentioned set of equations has been already studied in the literature, yielding some interesting results. According to the generalized Darboux transformation, Tian et al. [23] examined the rogue wave solutions of Eq. (1), and proposed that the second-order and four-petaled rogue waves were composed of a bright rogue wave and a four-petaled rogue wave, respectively. Xu et al. [24] carried out the Nth iterated Darboux transformation, and obtained the triple Wronskian solutions, while the interaction between inhomogeneous bright-bright solitons was analyzed. Wang et al. [25] explored the influence of the various parameters on the modulation instability of Eq. (1), and higher-order asymmetric breather and rogue wave solutions were also derived by performing the modified Darboux transformation. In another interesting work, Tian et al. [26] used the Lax pair of Eq. (1) to display the accuracy of one- and two-soliton solutions, and discussed the interaction of two neighboring solitons by using the split-step Fourier method. Li et al. [27] described the propagation properties of self-similar soliton optical pulses in coupled inhomogeneous optical fiber systems. Additionally, Musammil et al. [28] reported the exact phase dynamics of both bright and dark vector solitons and conducted an asymptotic analysis of two-soliton solutions by employing the Hirota bilinear method. In terms of Kadotsev–Peveashvili hierarchy simplification, Tian et al. [29] reported non-degenerate N-dark-dark soliton solutions. Han et al. [30] generated also the N-bright-dark soliton solutions through the Kadotsev–Pevyashvili hierarchy reduction, and the inelastic interaction between the bright-dark solitons was discovered. However, the dynamical characteristics of the localized waves in Eq. (1) have been scarcely reported in the literature. Along these lines, in this work, the localized wave solutions were explored by using the generalized Darboux transformation. The localized waves mainly consist of rogue waves, solitons and breathers, which include the interaction of rogue waves with solitons, and rogue waves interacted with breathers. Thus, a series of novel evolutionary plots were obtained, such as periodic, V-type, and K-type plots.

The structure of this work is organized as follows. In Sect. 2, the generalized Darboux transformation was derived and the iterative expression of the Nth order localized wave solutions were obtained. In Sect. 3, the evolutionary plots of the first- and second-order localized waves were drawn by performing numerical simulations, and their dynamical characteristics were analyzed. Finally, in Sect. 4, the conclusions are presented.

2 Generalized Darboux transformation

The following Lax pair of Eq. (1) was considered,

$$\Phi_t=U\Phi, \tag{2a}$$

$$\Phi_z=V\Phi, \tag{2b}$$

where

$$U=\begin{pmatrix} i\lambda & -\sqrt{\frac{\gamma(z)}{\beta(z)}}q_1^* & -\sqrt{\frac{\gamma(z)}{\beta(z)}}q_2^* \\ \sqrt{\frac{\gamma(z)}{\beta(z)}}q_1 & -i\lambda & 0 \\ \sqrt{\frac{\gamma(z)}{\beta(z)}}q_2 & 0 & -i\lambda \end{pmatrix},$$

$$V=\begin{pmatrix} i\lambda^2\beta(z)-\frac{i}{2}\left(|q_1|^2+|q_2|^2\right)\gamma(z) & \left(\frac{i}{2}q_{1t}^*-\lambda q_1^*\right)\beta(z)\sqrt{\frac{\gamma(z)}{\beta(z)}} & \left(\frac{i}{2}q_{2t}^*-\lambda q_2^*\right)\beta(z)\sqrt{\frac{\gamma(z)}{\beta(z)}} \\ \left(\frac{i}{2}q_{1t}+\lambda q_1\right)\beta(z)\sqrt{\frac{\gamma(z)}{\beta(z)}} & -i\lambda^2\beta(z)+\frac{i}{2}|q_1|^2\gamma(z) & \frac{i}{2}q_1q_2^*\gamma(z) \\ \left(\frac{i}{2}q_{2t}+\lambda q_2\right)\beta(z)\sqrt{\frac{\gamma(z)}{\beta(z)}} & \frac{i}{2}q_1^*q_2\gamma(z) & -i\lambda^2\beta(z)+\frac{i}{2}|q_2|^2\gamma(z) \end{pmatrix},$$

where λ is the spectral parameter, $\Phi=(\phi,\varphi,\chi)^T$ represents the vector solution of Eq. (2), and the superscript T denotes the transpose for a vector. It is easy to verify that U and V satisfy the following compatibility condition: $U_z-V_t+UV-VU=0$.

The Darboux matrix J can be formulated as follows:

$$J=\lambda I-H\Lambda H^{-1}, \tag{3}$$

where

$$H=\begin{pmatrix}\phi_1 & \varphi_1^* & \chi_1^* \\ \varphi_1 & -\phi_1^* & 0 \\ \chi_1 & 0 & -\phi_1^*\end{pmatrix},\ \Lambda=\begin{pmatrix}\lambda_1 & 0 & 0 \\ 0 & \lambda_1^* & 0 \\ 0 & 0 & \lambda_1^*\end{pmatrix}.$$

where $\Phi=(\phi_1,\varphi_1,\chi_1)^T$ refers to the eigenfunction of Eq. (2) corresponding to the spectral parameters $\lambda=\lambda_1$ and seed solutions $q_1=q_1[0]$ and $q_2=q_2[0]$. Thus, the classical Darboux transformation can be defined as follows:

$$\lambda=\lambda_k,\ \Phi_k=(\phi_k,\varphi_k,\chi_k)^T,\ (k=1,2,\ldots,N), \tag{4}$$

$$\Phi_N[N-1]=J[N-1]J[N-2]\cdots J[1]\Phi_N, \tag{5}$$

$$\begin{aligned} q_1[N]&=q_1[0] \\ &-2i\sqrt{\frac{\beta(z)}{\gamma(z)}}\sum_{k=1}^{N}\left(\lambda_1-\lambda_1^*\right) \\ &\frac{\phi_k^*[k-1]\varphi_k[k-1]}{|\phi_k[k-1]|^2+|\varphi_k[k-1]|^2+|\chi_k[k-1]|^2}, \end{aligned} \tag{6a}$$

$$\begin{aligned} q_2[N]&=q_2[0] \\ &-2i\sqrt{\frac{\beta(z)}{\gamma(z)}}\sum_{k=1}^{N}\left(\lambda_1-\lambda_1^*\right) \\ &\frac{\phi_k^*[k-1]\chi_k[k-1]}{|\phi_k[k-1]|^2+|\varphi_k[k-1]|^2+|\chi_k[k-1]|^2}, \end{aligned} \tag{6b}$$

where

$$\begin{aligned} J[k]&=\lambda_{k+1}I-H[k-1]\Lambda[k]H[k-1]^{-1}, \\ \Phi_k[k-1]&=(J[k-1]J[k-2]\cdots J[1])\big|_{\lambda=\lambda_k}\Phi_k, \\ H[k-1]&=\begin{pmatrix}\phi_k[k-1] & \varphi_k^*[k-1] & \chi_k^*[k-1] \\ \varphi_k[k-1] & -\phi_k^*[k-1] & 0 \\ \chi_k[k-1] & 0 & -\phi_k^*[k-1]\end{pmatrix}, \\ \Lambda[k]&=\begin{pmatrix}\lambda_k & 0 & 0 \\ 0 & \lambda_k^* & 0 \\ 0 & 0 & \lambda_k^*\end{pmatrix}. \end{aligned}$$

Based on the above-mentioned classical Darboux transformation, the generalized Darboux transformation of Eq. (1) can be carried out. By assuming that $\Phi_1=\Phi_1(\lambda_1,\eta)$ is a solution of Eq. (2) and η denotes a small parameter, the following Taylor expansion of $\eta=0$ can be obtained:

$$\Phi_1=\Phi_1^{[0]}+\Phi_1^{[1]}\eta+\Phi_1^{[2]}\eta^2+\cdots+\Phi_1^{[N]}\eta^N+o\left(\eta^N\right), \tag{7}$$

where

$$\Phi_1^{[k]}=\frac{1}{k!}\frac{\partial^k}{\partial\lambda^k}\Phi_1(\lambda)|_{\lambda=\lambda_1}=\left(\phi_1^{[k]},\varphi_1^{[k]},\chi_1^{[k]}\right)^T,\ (k=0,1,2,\ldots,N).$$

It can be easily confirmed that $\Phi_1^{[0]}=\Phi_1[0]$ is a special solution with $\lambda=\lambda_1$, $q_1=q_1[0]$, and $q_2=q_2[0]$ of Eq. (2). Therefore, the generalized Darboux transformation of Nth order can be defined as follows:

$$\begin{aligned} \Phi_1[N-1]=\Phi_1^{[0]}&+\left[\sum_{l=1}^{N-1}J_1[l]\right]\Phi_1^{[1]} \\ &+\left[\sum_{l=1}^{N-1}\sum_{h>l}^{N-1}J_1[h]J_1[l]\right]\Phi_1^{[2]} \\ &+\cdots+\left[J_1[N-1]\cdots J_1[2]J_1[1]\right]\Phi_1^{[N-1]}, \end{aligned} \tag{8}$$

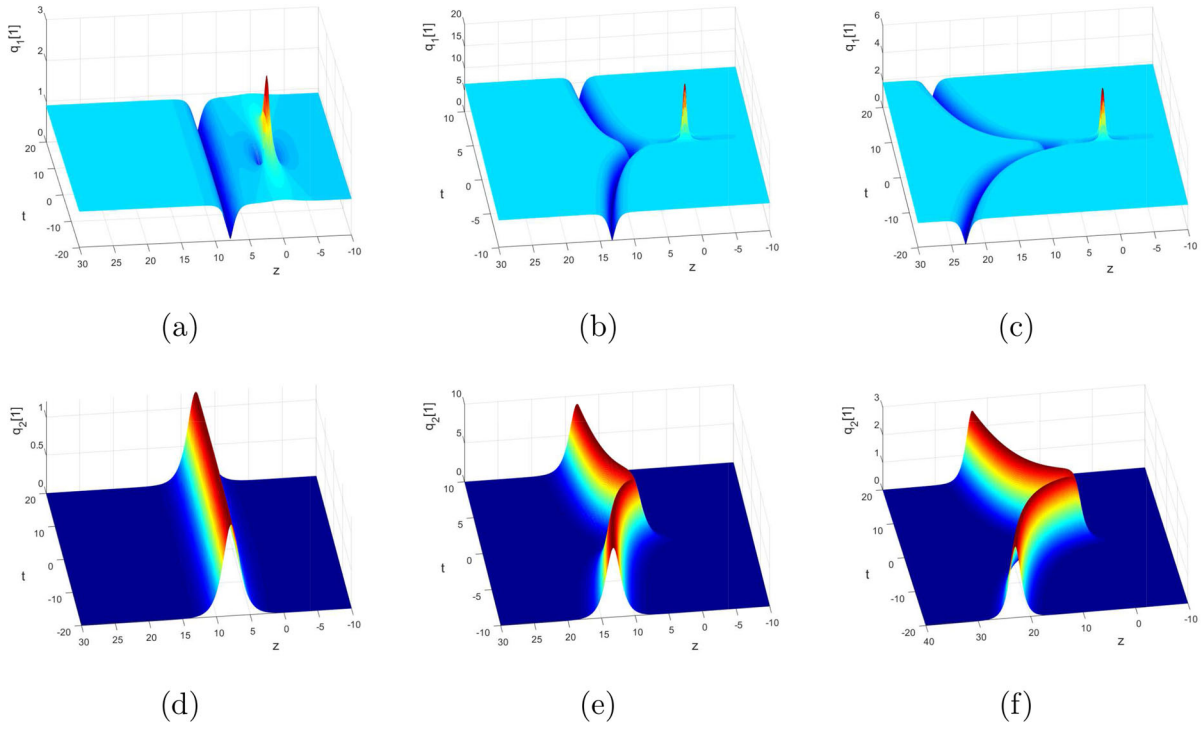

Fig. 1 Depiction of the first-order localized waves with $d_1 = 1, d_2 = 0, \alpha = \frac{1}{100}$ and **a**, **d** $\beta(z) = \frac{1}{5}, \gamma(z) = \frac{1}{4}$; **b**, **e** $\beta(z) = 20z, \gamma(z) = \frac{z}{2}$; **c**, **f** $\beta(z) = 10z^4, \gamma(z) = 3z^4$

$$q_1[N] = q_1[N-1] - 2i\sqrt{\frac{\beta(z)}{\gamma(z)}}(\lambda_1 - \lambda_1^*) \frac{\phi_1^*[N-1]\varphi_1[N-1]}{|\phi_1[N-1]|^2 + |\varphi_1[N-1]|^2 + |\chi_1[N-1]|^2}, \tag{9a}$$

$$q_2[N] = q_2[N-1] - 2i\sqrt{\frac{\beta(z)}{\gamma(z)}}(\lambda_1 - \lambda_1^*) \frac{\phi_1^*[N-1]\chi_1[N-1]}{|\phi_1[N-1]|^2 + |\varphi_1[N-1]|^2 + |\chi_1[N-1]|^2}, \tag{9b}$$

where

$$J_1[k] = \lambda_1 I - H_1[k-1]\Lambda_1 H_1[k-1]^{-1},$$
$$\Phi_1[N-1] = (\varphi_1[N-1], \chi_1[N-1], \phi_1[N-1])^T,$$
$$H_1[k-1] = \begin{pmatrix} \phi_1[k-1] & \varphi_1^*[k-1] & \chi_1^*[k-1] \\ \varphi_1[k-1] & -\phi_1^*[k-1] & 0 \\ \chi_1[k-1] & 0 & -\phi_1^*[k-1] \end{pmatrix},$$
$$\Lambda_1 = \begin{pmatrix} \lambda_1 & 0 & 0 \\ 0 & \lambda_1^* & 0 \\ 0 & 0 & \lambda_1^* \end{pmatrix}.$$

3 Localized wave solutions

By assuming that $q_1[0] = d_1\sqrt{\frac{\beta(z)}{\gamma(z)}}e^{i\omega(z)}$ and $q_2[0] = d_2\sqrt{\frac{\beta(z)}{\gamma(z)}}e^{i\omega(z)}$ are the seed solutions of the localized waves, where $\omega(z) = \left(d_1^2 + d_2^2\right)\int \beta(z)\,dz$, d_1 and d_2 stand for the arbitrary real constants. The corresponding basic vector solution at $\lambda = \left(i\sqrt{d_1^2 + d_2^2}\right)\left(1 + \eta^2\right)$ can be obtained as below:

$$\Phi_1(\eta) = \begin{pmatrix} \left(C_1 e^{M_1+M_2} - C_2 e^{M_1-M_2}\right) e^{-\frac{i\omega(z)}{2}} \\ \rho_1\left(C_1 e^{M_1-M_2} - C_2 e^{M_1+M_2}\right) e^{\frac{i\omega(z)}{2}} + \alpha d_2 e^{M_3} \\ \rho_2\left(C_1 e^{M_1-M_2} - C_2 e^{M_1+M_2}\right) e^{\frac{i\omega(z)}{2}} - \alpha d_1 e^{M_3} \end{pmatrix}, \tag{10}$$

where

$$C_1 = \frac{\sqrt{\lambda + \sqrt{\lambda^2 + d_1^2 + d_2^2}}}{\sqrt{\lambda^2 + d_1^2 + d_2^2}}, C_2 = \frac{\sqrt{\lambda - \sqrt{\lambda^2 + d_1^2 + d_2^2}}}{\sqrt{\lambda^2 + d_1^2 + d_2^2}},$$

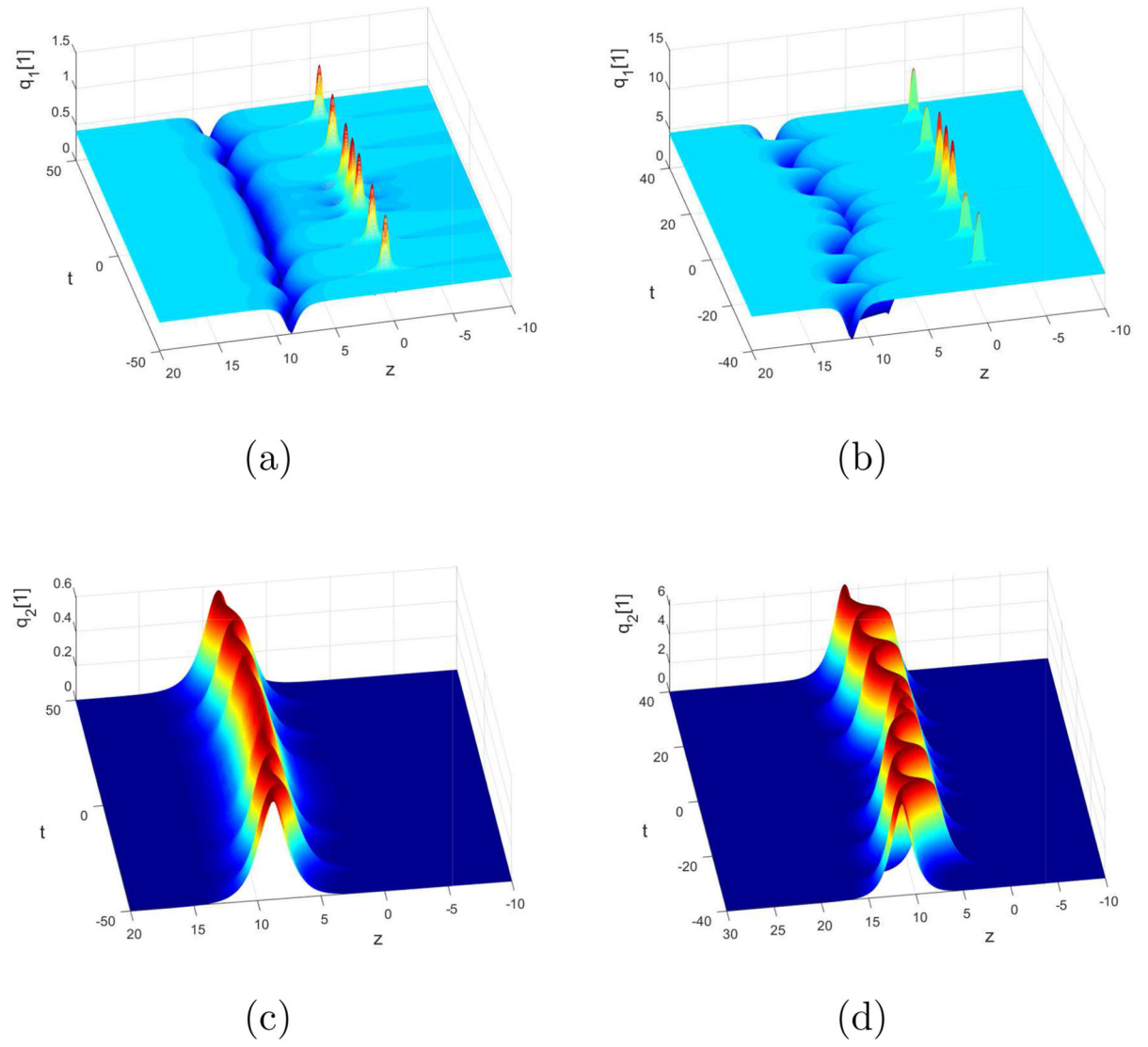

Fig. 2 Depiction of the first-order localized waves with $d_1 = 1, d_2 = 0, \alpha = \frac{1}{100}$ and **a**, **c** $\beta(z) = \frac{1}{2}\cos\left(\frac{z}{5}\right), \gamma(z) = 3\cos\left(\frac{z}{5}\right)$; **b**, **d** $\beta(z) = 10\cos\left(\frac{z}{4}\right), \gamma(z) = \frac{1}{2}\cos\left(\frac{z}{4}\right)$

$$M_1 = 0, M_2 = i\sqrt{\lambda^2 + d_1^2 + d_2^2}\,(t + \lambda\beta(z)\,z + \Omega(\eta)),$$
$$M_3 = -i\lambda\,(t + \lambda\beta(z)\,z),$$
$$\rho_1 = \frac{d_1}{\sqrt{d_1^2 + d_2^2}}, \rho_2 = \frac{d_2}{\sqrt{d_1^2 + d_2^2}},$$
$$\Omega(\eta) = \sum_{j=1}^{N}\left(m_j + in_j\right)\eta^{2j},$$

where α, m_j, and n_j are arbitrary real constants. $\Phi_1(\eta)$ can be expanded at $\eta = 0$ by using the Taylor series as follows:

$$\Phi_1(\eta) = \Phi_1^{[0]} + \Phi_1^{[1]}\eta^2 + \Phi_1^{[2]}\eta^4 + \Phi_1^{[3]}\eta^6 + \cdots, \quad (11)$$

where

$$\Phi_1(\eta) = \left(\phi_1^{[k]}, \varphi_1^{[k]}, \chi_1^{[k]}\right)^T = \frac{1}{(2k)!}\frac{\partial^{2k}\Phi_1}{\partial\eta^{2k}}\bigg|_{\eta=0},$$
$$(k = 0, 1, 2, \ldots).$$

Owing to the expression $\Phi_1^{[j]} = \left(\phi_1^{[j]}, \varphi_1^{[j]}, \chi_1^{[j]}\right)^T$ $(j = 1, 2, \ldots)$ is complex, its specific form was omitted. Furthermore, the first- and second-order localized wave solutions of Eq. (1) were discussed, and the

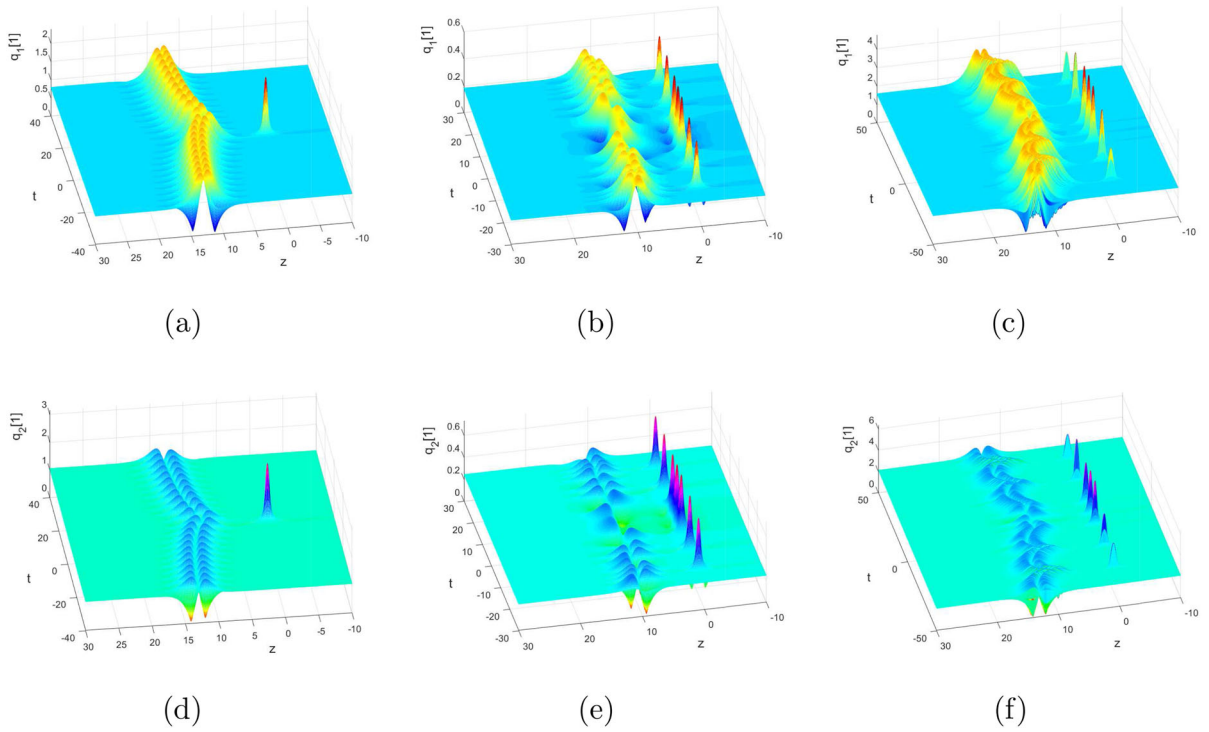

Fig. 3 Depiction of the first-order localized waves with $d_1 = \frac{1}{2}, d_2 = \frac{2}{3}, \alpha = \frac{1}{100}$ and **a**, **d** $\beta(z) = 5, \gamma(z) = 2$; **b**, **e** $\beta(z) = \frac{2}{3}\cos\left(\frac{z}{3}\right), \gamma(z) = 5\cos\left(\frac{z}{3}\right)$; **c**, **f** $\beta(z) = 5\cos\left(\frac{z}{5}\right), \gamma(z) = \frac{1}{2}\cos\left(\frac{z}{5}\right)$

dynamical characteristics of localized waves were analyzed by evolutionary plots.

Obviously, when $\lambda = \lambda_1$, $q_1 = q_1[0]$, and $q_2 = q_2[0]$, $\Phi_1^{[0]} = \left(\phi_1^{[0]}, \varphi_1^{[0]}, \chi_1^{[0]}\right)^T$ is the solution of the Lax pair. According to Eqs. (8) and (9), the first-order localized wave solutions of Eq. (1) can be obtained as follows:

$$q_1[1] = q_1[0] - 2i\sqrt{\frac{\beta(z)}{\gamma(z)}}\left(\lambda_1 - \lambda_1^*\right)\frac{\phi_1^*[0]\varphi_1[0]}{|\phi_1[0]|^2 + |\varphi_1[0]|^2 + |\chi_1[0]|^2}, \tag{12a}$$

$$q_2[1] = q_2[0] - 2i\sqrt{\frac{\beta(z)}{\gamma(z)}}\left(\lambda_1 - \lambda_1^*\right)\frac{\phi_1^*[0]\chi_1[0]}{|\phi_1[0]|^2 + |\varphi_1[0]|^2 + |\chi_1[0]|^2}. \tag{12b}$$

The evolutionary plots of the first-order localized waves were derived by altering values of the free parameters $d_1, d_2, \alpha, \beta(z)$, and $\gamma(z)$. Then, the dynamics of the first-order localized waves were analyzed.

Figure 1 depicts the interaction between the first-order rogue waves and the bright-dark solitons. As can be observed, when $\beta(z)$ and $\gamma(z)$ were both selected as constants, the propagation direction of the dark soliton in the component $q_1[1]$ was parallel to the t-axis, as shown in Fig. 1a. On the contrary, when $\beta(z)$ and $\gamma(z)$ were variable coefficients, as can be seen in Fig. 1b, the dark soliton in the component $q_1[1]$ bent at $t = 0$. When $\beta(z) = 10z^4$ and $\gamma(z) = 3z^4$, the curvature of the dark soliton was more pronounced and exhibited the shape of V, as displayed in Fig. 1c. In the zero-amplitude background, only a bright soliton can be found in the component $q_2[1]$, while the first-order rogue waves can not easily detected, as shown in Fig. 1d–f.

When trigonometric functions were assigned to both $\beta(z)$ and $\gamma(z)$, the evolutionary figures of the first-order periodic rogue waves interacting with periodic bright-dark solitons were obtained in Fig. 2. By comparing Fig. 2a, b, it was found that due to the influence of the parameters $\beta(z)$ and $\gamma(z)$, the periodic change of the dark soliton in the component $q_1[1]$ was more pronounced when $\beta(z) = 10\cos\left(\frac{z}{4}\right)$ and $\gamma(z) = \frac{1}{2}\cos\left(\frac{z}{4}\right)$. Only one periodic bright soliton can be also seen in the component $q_2[1]$, as illustrated in Fig. 2c, d.

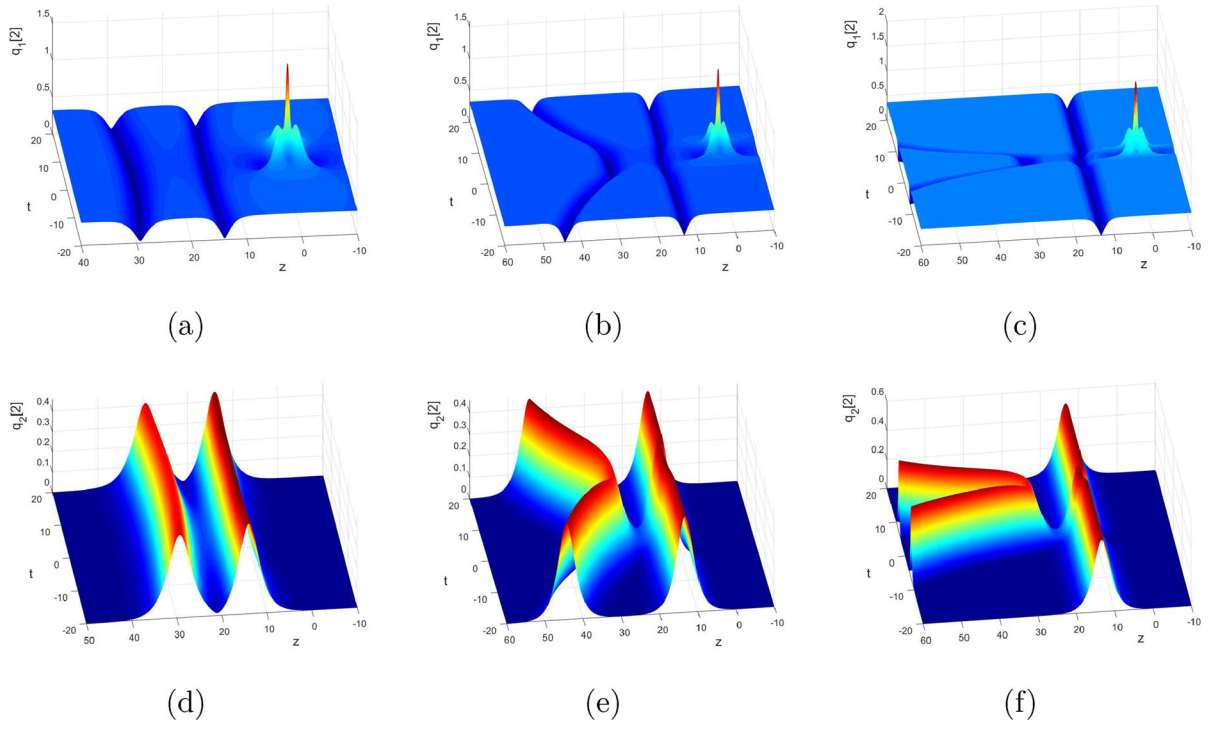

Fig. 4 Depiction of the second-order localized waves with $d_1 = \frac{1}{2}, d_2 = 0, \alpha = \frac{1}{100}, m_1 = 0, n_1 = 0$ and **a**, **d** $\beta(z) = 2, \gamma(z) = 5$; **b**, **e** $\beta(z) = 2z, \gamma(z) = 5z$; **c**, **f** $\beta(z) = 5z^3, \gamma(z) = 10z^3$

Figure 3 depicts the collision of the first-order rogue waves with breathers. By both $\beta(z)$ and $\gamma(z)$ were selected as constants, the interaction between the first-order rogue waves and a breather was illustrated. Figure 3a, d present that the amplitude of $q_1[1]$ is higher than the amplitude of the component $q_2[1]$, which is affected by the parameters d_1 and d_2. When $\beta(z)$ and $\gamma(z)$ were trigonometric functions, the periodic rogue waves interacted with the first-order breather, and the breather propagation direction was parallel to the t-axis, as shown in Fig. 3b, e. Moreover, when $\beta(z) = 5\cos\left(\frac{z}{5}\right)$ and $\gamma(z) = \frac{1}{2}\cos\left(\frac{z}{5}\right)$, the evolutionary plots of the interaction between the periodic rogue waves and periodic breathers were obtained in Fig. 3c, f.

Based on the following limit formula

$$\begin{aligned}\Phi_1[1] &= \lim_{\eta\to 0}\frac{J[1]|_{\lambda=\lambda_1(1+\eta^2)}\Phi_1}{\eta^2}\\ &= \lim_{\eta\to 0}\frac{\left(\lambda_1\eta^2 + J_1[1]|_{\lambda=\lambda_1}\right)\Phi_1}{\eta^2}\\ &= \lambda_1\Phi_1^{[0]} + J[1]\,\Phi_1^{[1]},\end{aligned} \tag{13}$$

and according to the first-order localized wave solutions and the generalized Darboux transformation, the iterative expression of the second-order localized wave solutions of Eq. (1) are as follows,

$$\begin{aligned}q_1[2] &= q_1[1]\\ &\quad -2i\sqrt{\frac{\beta(z)}{\gamma(z)}}\left(\lambda_1-\lambda_1^*\right)\frac{\phi_1^*[1]\,\varphi_1[1]}{|\phi_1[1]|^2+|\varphi_1[1]|^2+|\chi_1[1]|^2},\end{aligned} \tag{14a}$$

$$\begin{aligned}q_2[2] &= q_2[1]\\ &\quad -2i\sqrt{\frac{\beta(z)}{\gamma(z)}}\left(\lambda_1-\lambda_1^*\right)\frac{\phi_1^*[1]\,\chi_1[1]}{|\phi_1[1]|^2+|\varphi_1[1]|^2+|\chi_1[1]|^2}.\end{aligned} \tag{14b}$$

Furthermore, the dynamical characteristics of the second-order localized wave solutions were analyzed by altering different values for the free parameters d_1, d_2, α, m_1, n_1, $\beta(z)$, and $\gamma(z)$.

Similar to Fig. 1, Fig. 4 depicts the interaction of the second-order rogue waves and the bright-dark solitons. When $\beta(z)$ and $\gamma(z)$ were taken as constants, the propagation direction of the bright-dark solitons in components $q_1[2]$ and $q_2[2]$ was parallel to the

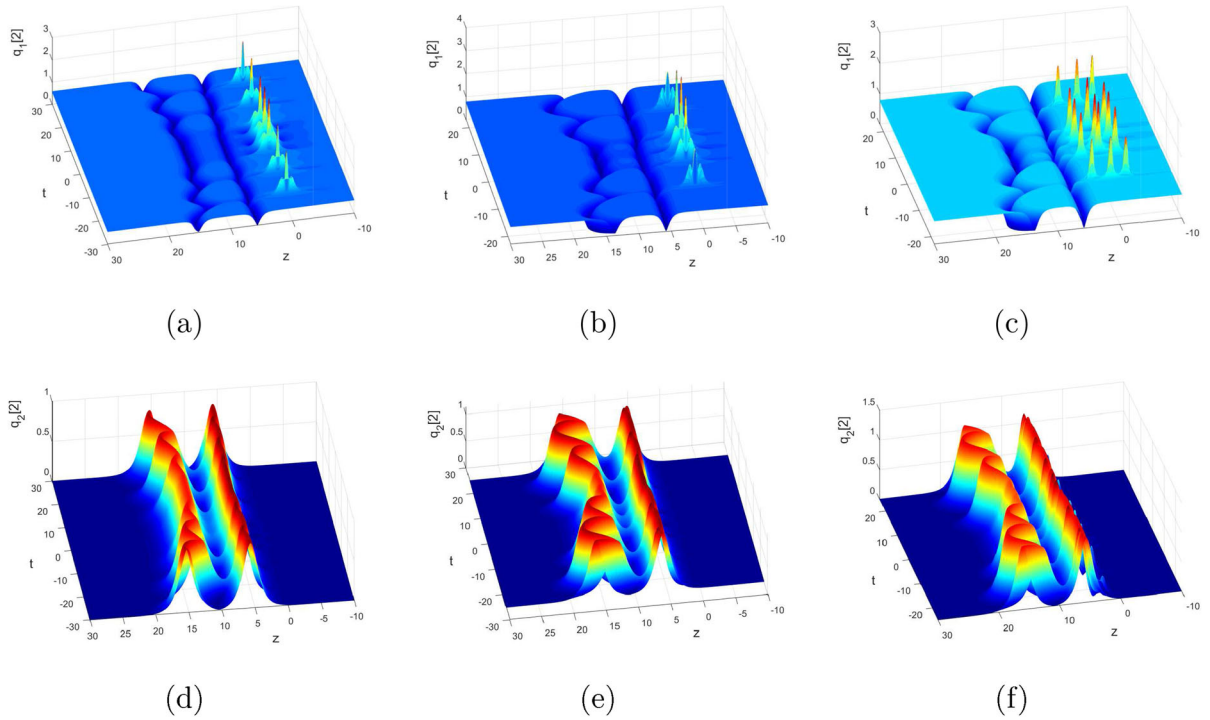

Fig. 5 Depiction of the second-order localized waves with $d_1 = 1, d_2 = 0, \alpha = \frac{1}{100}$ and **a**, **d** $\beta(z) = \cos\left(\frac{z}{3}\right), \gamma(z) = 3\cos\left(\frac{z}{3}\right), m_1 = 0, n_1 = 0$; **b**, **e** $\beta(z) = 3\cos\left(\frac{z}{3}\right), \gamma(z) = 5\cos\left(\frac{z}{3}\right), m_1 = 0, n_1 = 0$; **c**, **f** $\beta(z) = 3\cos\left(\frac{z}{3}\right), \gamma(z) = 5\cos\left(\frac{z}{3}\right), m_1 = 3, n_1 = 20$

t-axis, as can be observed in Fig. 4a, d. When $\beta(z)$ and $\gamma(z)$ were assumed as linear functions, the bright-dark solitons exhibited the shape of K, and the second-order rogue waves appeared at $t = 0$, as shown in Fig. 4b, e. Besides, by considering that $\beta(z) = 5z^3$ and $\gamma(z) = 10z^3$, it was found that one of the solitons propagated along with the t-axis and the velocity remained constant, and the other soliton took the V-shaped depicted in Fig. 4c, f. Figure 4d–f display also that the second-order rogue waves in component q_2 [2] are difficult to be identified under the influence of the zero-amplitude background.

Figure 5 illustrates the dynamical characteristics of the second-order rogue waves and bright-dark solitons when $\beta(z)$ and $\gamma(z)$ are trigonometric functions. By assuming that $\beta(z) = \cos\left(\frac{z}{3}\right)$ and $\gamma(z) = 3\cos\left(\frac{z}{3}\right)$, the periodic rogue waves interacted with two periodic dark solitons, as shown in Fig. 5a. If the other parameters remain unchanged, it was found that the period of bright-dark soliton decreased and the propagation velocity became faster by increasing $\beta(z)$ and $\gamma(z)$, as shown in Fig. 5b, e. In addition, as the values of the parameters m_1 and n_1 changed, the periodic rogue waves were separated, as can be ascertained by comparing Fig. 5b, e and c, f.

When neither d_1 nor d_2 had a value of zero, whereas $\beta(z)$ and $\gamma(z)$ were variable coefficients, the components q_1 [2] and q_2 [2] exhibited the same structure. Figure 6 demonstrated the second-order rogue waves coexisted with two breathers, and the breathers were arranged in the K-shaped. When $m_1 = 20$ and $n_1 = 3$, the second-order rogue waves in the components q_1 [2] and q_2 [2] were separated into three first-order rogue waves, as shown in Fig. 6b, d.

In Fig. 7, the dynamical characteristics of the second-order periodic rogue waves with two breathers are systematically studied when $\beta(z)$ and $\gamma(z)$ are trigonometric functions. By considering that $\beta(z) = \frac{1}{2}\cos\left(\frac{z}{4}\right)$ and $\gamma(z) = 5\cos\left(\frac{z}{4}\right)$, the second-order periodic rogue waves interacted with two breathers, which were parallel to the t-axis, as shown in Fig. 7a, d. If the other parameters were left unchanged, the second-

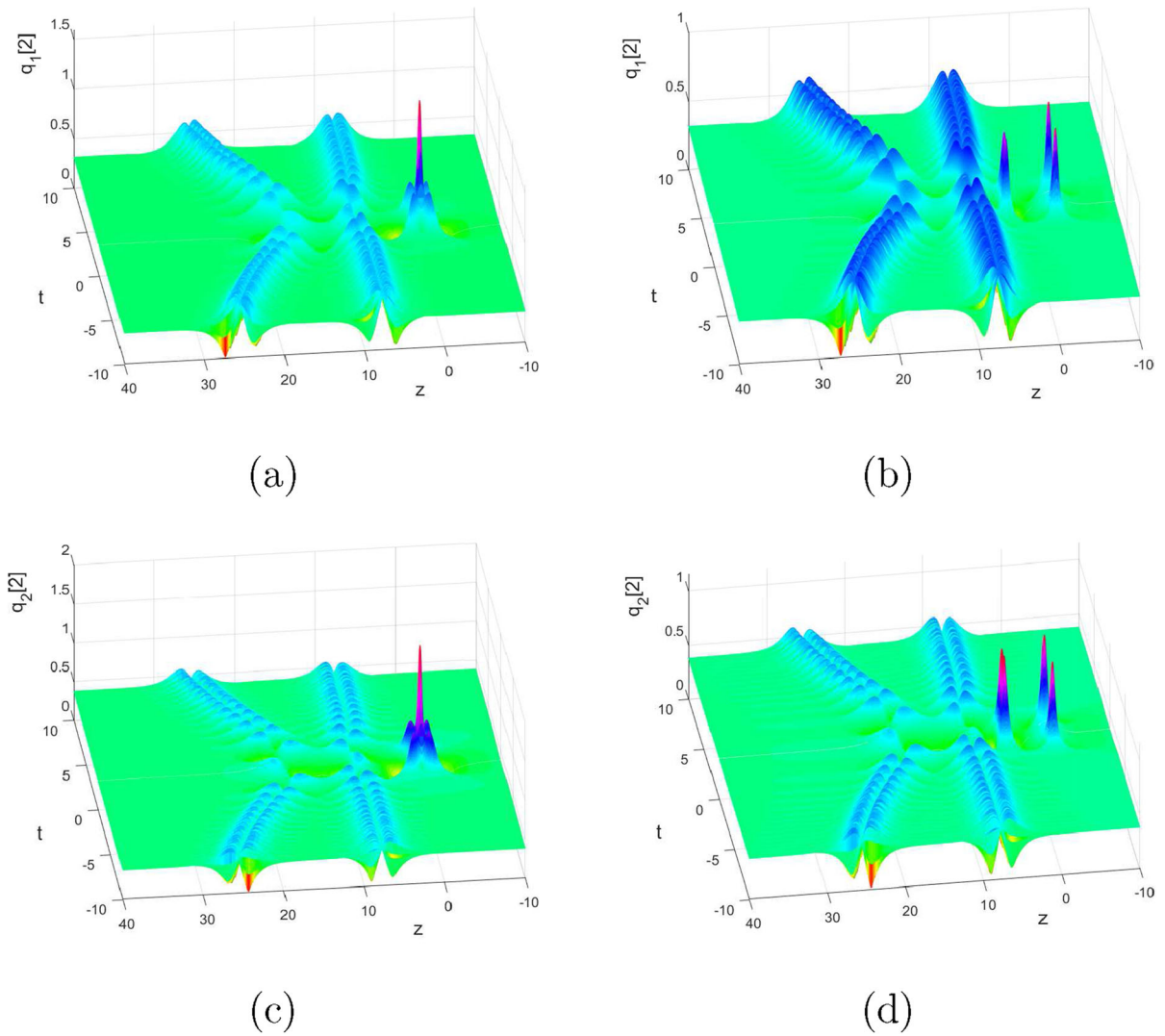

Fig. 6 Depiction of the second-order localized waves with $d_1 = \frac{1}{2}, d_2 = \frac{3}{5}, \alpha = \frac{1}{100}, \beta(z) = 2z, \gamma(z) = 5z$ and **a**, **c** $m_1 = 0, n_1 = 0$; **b**, **d** $m_1 = 20, n_1 = 3$

order periodic rogue waves in the components q_1 [2] and q_2 [2] were separated in Fig. 7b, e when the separation parameters m_1 and n_1 were not equal to zero. When $\beta(z) = 5\cos\left(\frac{z}{3}\right)$ and $\gamma(z) = 4\cos\left(\frac{z}{3}\right)$, the interaction between the second-order periodic rogue waves and two periodic breathers is affected. More specifically, one of them is changed from parallel to the t-axis to an arc-like line and symmetrical with respect to $t = 0$, as seen in Fig. 7c, f.

4 Conclusions

In this work, the localized waves of a variable-coefficient coupled NLS equation were thoroughly investigated. On the basis of the classical Darboux transformation, the generalized Darboux transformation was derived by using the Taylor expansion formula. Then, according to the generalized Darboux transformation, the first- and second-order localized wave solutions were obtained. Furthermore, the localized wave evolutionary plots of the variable-coefficient coupled NLS equation were derived by performing numerical

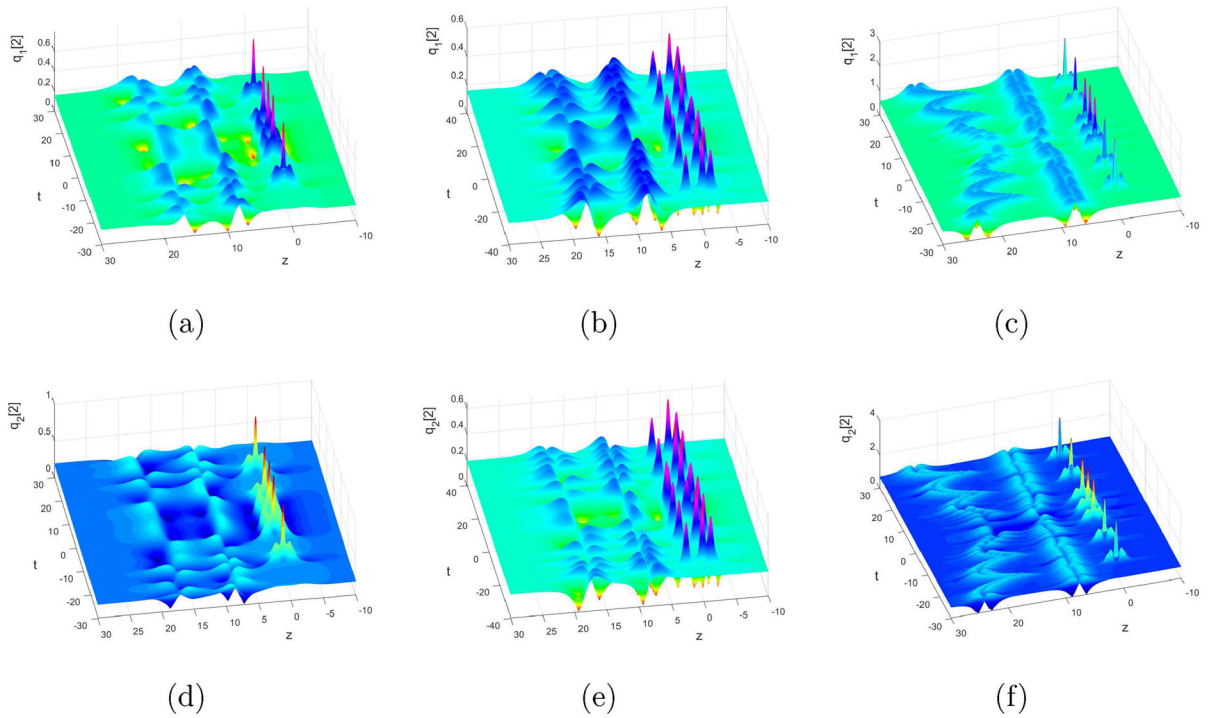

Fig. 7 Depiction of the second-order localized waves with $d_1 = \frac{1}{2}, d_2 = \frac{3}{5}, \alpha = \frac{1}{100}$ and **a**, **d** $\beta(z) = \frac{1}{2}\cos\left(\frac{z}{4}\right), \gamma(z) = 5\cos\left(\frac{z}{4}\right), m_1 = 0, n_1 = 0$; **b**, **e** $\beta(z) = \frac{1}{2}\cos\left(\frac{z}{4}\right), \gamma(z) = 5\cos\left(\frac{z}{4}\right), m_1 = 2, n_1 = 3$; **c**, **f** $\beta(z) = 5\cos\left(\frac{z}{3}\right), \gamma(z) = 4\cos\left(\frac{z}{3}\right), m_1 = 0, n_1 = 0$

simulations, and their dynamical characteristics were analyzed. From our analysis, it was demonstrated that the variable coefficients $\beta(z)$ and $\gamma(z)$ directly affect the shape of the localized waves. Particularly, when $\beta(z)$ and $\gamma(z)$ were constant, the common localized waves occurred. In striking contrast, when $\beta(z)$ and $\gamma(z)$ were primary functions or higher-order exponential functions, the rogue waves interacted with the V-shaped or K-shaped solitons and breathers, while the degree of curvatures of the solitons or breathers was more obvious as the exponential number increases. When $\beta(z)$ and $\gamma(z)$ were trigonometric functions, the localized waves exhibited significant periodicity when propagating along with the t-axis. Our results might provide valuable insights for studying the propagation of localized waves in an inhomogeneous optical fiber. In the future, it is hoped that the high-order localized wave evolutionary plots of the variable-coefficient coupled NLS equation can be obtained, which will further enrich the research of the localized waves.

Funding The authors sincerely thanks for the support of the National Natural Science Foundation of China (NNSFC) through grant Nos. 11602232, Shanxi Natural Science Foundation (SNSF) through grant Nos. 202203021211086 and Nos. 202203021211088 and Shanxi Province Research Funding Program for Returning Students (2022-150).

Data availability Data sharing does not apply to this article as no data sets were generated or analyzed during the current study.

Declarations

Conflict of interest The authors declare that they have no conflicts of interest to report regarding the present study.

References

1. Xu, C.X., Xu, T., Meng, D.X., et al.: Binary Darboux transformation and new soliton solutions of the focusing nonlocal nonlinear Schrödinger equation. J. Math. Anal. Appl. **516**(2), 126514 (2022)
2. Li, L., Wang, L., Yu, F.J.: Some general bright soliton solutions and interactions for a (2+1)-dimensional nonlocal nonlinear Schrödinger equation. Appl. Math. Lett. **141**, 108600 (2023)
3. Yang, J., Tian, H.J.: Nth-order smooth positon and breather-positon solutions for the generalized integrable discrete non-

linear Schrödinger equation. Nonlinear Dyn. **111**(6), 5629–5639 (2022)
4. Ndogmo, J.C.: Group classification and exact solutions of a class of nonlinear waves. Appl. Math. Comput. **443**, 127769 (2023)
5. Triki, H., Sun, Y.Z., Zhou, Q., et al.: Dark solitary pulses and moving fronts in an optical medium with the higher-order dispersive and nonlinear effects. Chaos Solitons Fract.: Interdiscip. J. Nonlinear Sci. Nonequilibrium Complex Phenomena **164**, 112622 (2022)
6. Turbiner, A.V., Shuryak, E.: On the connection between perturbation theory and new semiclassical expansion in quantum mechanics. Nucl. Phys. Sect. B **989**, 116117 (2023)
7. Fioravanti, D., Rossi, M.: On the origin of the correspondence between classical and quantum integrable theories. Phys. Lett. B **838**, 137706 (2023)
8. Liu, Y., Cui, T., Li, D.: Emerging d-d orbital coupling between non-d-block main-group elements Mg and I at high pressure. iScience **26**(3), 106113–106113 (2023)
9. Sun, L., Zhang, J.W., Zhou, G., et al.: Theoretical investigations of weakly- and strongly-coupled multi-core fibers for the applications of optical submarine communications under power and fiber count limits. Opt. Express **31**(3), 4615–4629 (2023)
10. Jin, T.W., Yi, X.W., Lin, H.: Phase rearrangement shell mapping in single-span nonlinear optical fiber communication system. Opt. Commun. **530**, 129107 (2023)
11. Le, X., Kong, Y., Han, L.J.: Solutions of solitary-wave for the variable-coefficient nonlinear Schrödinger equation with two power-law nonlinear terms. Int. J. Mod. Phys. B **32**(28), 11 (2018)
12. Jia, R.R., Wang, Y.F.: Dark soliton solutions for the coupled variable-coefficient fourth-order nonlinear Schrödinger equations in the inhomogeneous optical fiber. Wave Motion **114**, 103042 (2022)
13. Mathanaranjan, T.: Optical solitons and stability analysis for the new (3+1)-dimensional nonlinear Schrödinger equation. J. Nonlinear Opt. Phys. Mater. **32**(02).https://doi.org/10.1142/S0218863523500169 (2023)
14. Zhou, H.J., Chen, Y.: High-order soliton solutions and their dynamics in the inhomogeneous variable coefficients Hirota equation. Commun. Nonlinear Sci. Numer. Simul. **120**, 107149 (2023)
15. Shi, W., Zha, Q.L.: Higher-order mixed solution and breather solution on a periodic background for the Kundu equation. Commun. Nonlinear Sci. Numer. Simul. **119**, 107134 (2023)
16. Zhen, Y.P.: Rogue waves on the periodic background in the extended mKdV equation. Eur. Phys. J. B **96**, 20 (2023)
17. Wu, X.H., Gao, Y.T.: Generalized Darboux transformation and solitons for the Ablowitz–Ladik equation in an electrical lattice. Appl. Math. Lett. **137**, 108476 (2023)
18. Ding, C.C., Gao, Y.T., Yu, X.: N-fold generalized Darboux transformation and breather-rogue waves on the constant/periodic background for a generalized mixed nonlinear Schrödinger equation. Nonlinear Dyn. **109**(2), 989–1004 (2022)
19. Zhang, J.Y., Zhu, M.K., Liu, S.L.: Bäcklund transformation, Lax pair, infinite conservation laws and exact solutions to a generalized (2+1)-dimensional equation. Int. J. Mod. Phys. B **36**(23), 2250146 (2022)
20. Ali Mohamed, R., Khattab Mahmoud, A., Mabrouk, S.M.: Optical soliton solutions for the integrable Lakshmanan–Porsezian–Daniel equation via the inverse scattering transformation method with applications. Optik **272**, 170256 (2023)
21. Yan, X.Y., Liu, J.Z., Xin, X.P.: Soliton solutions and lump-type solutions to the (2+1)-dimensional Kadomtsev–Petviashvili equation with variable coefficient. Phys. Lett. A **457**, 128574 (2023)
22. Wang, H.F., Zhang, Y.F.: Application of Riemann–Hilbert method to an extended coupled nonlinear Schrödinger equations. J. Comput. Appl. Math. **420**, 114812 (2023)
23. Yang, D.Y., Tian, B., Shen, Y.: Generalized Darboux transformation and rogue waves for a coupled variable-coefficient nonlinear Schrödinger system in an inhomogeneous optical fiber. Chin. J. Phys. **82**, 182–193 (2023)
24. Liang, J.W., Xu, T., Tang, M.Y., et al.: Integrable conditions and inhomogeneous soliton solutions of a coupled nonlinear Schrödinger system with distributed coefficients. Nonlinear Anal. Real World Appl. **14**(1), 329–339 (2013)
25. Wang, L., Zhang, L.L., Zhu, Y.J.: Modulational instability, nonautonomous characteristics and semirational solutions for the coupled nonlinear Schrödinger equations in inhomogeneous fibers. Commun. Nonlinear Sci. Numer. Simul. **40**, 216–237 (2016)
26. Tian, J.P., Li, J.H., Kang, L.S., et al.: Soliton solutions and soliton interactions for the coupled nonlinear Schrödinger equation with varying coefficients. Phys. Scr. **72**(5), 394–398 (2005)
27. Li, H.J., Tian, J.P., Song, L.J., et al.: Self-similar soliton-like beam generation and propagation in inhomogeneous coupled optical fiber media system. Opt.-Int. J. Light Electron Opt. **124**(24), 7040–7043 (2013)
28. Musammil, N.M., Subha, P.A., Nithyanandan, K., et al.: Phase dynamics of inhomogeneous Manakov vector solitons. Phys. Rev. E **100**(11), 012213 (2019)
29. Liu, L., Tian, B., Wu, X.Y.: Vector dark solitons for a coupled nonlinear Schrödinger system with variable coefficients in an inhomogeneous optical fiber. Z. für Naturforschung A **72**(8), 779–787 (2017)
30. Han, Y., Tian, B., Yuan, Y.Q., et al.: Bilinear forms and bright-dark solitons for a coupled nonlinear Schrödinger system with variable coefficients in an inhomogeneous optical fiber. Chin. J. Phys. **62**, 202–212 (2019)